Available online at www.sciencedirect.com
ScienceDirect
Journal of Luminescence 127 (2007) 116–128
JOURNAL OF LUMINESCENCE
www.elsevier.com/locate/jlumin

Ultra-wideband spectral analysis using S2 technology

R. Krishna Mohan[a,*], T. Chang[a], M. Tian[a,b], S. Bekker[a], A. Olson[a], C. Ostrander[a], A. Khallaayoun[a], C. Dollinger[a], W.R. Babbitt[a,b], Z. Cole[a,c], R.R. Reibel[a,c], K.D. Merkel[a,c], Y. Sun[b], R. Cone[b], F. Schlottau[d], K.H. Wagner[d]

[a]*Spectrum Lab, Montana State University, Bozeman, MT 59717, USA*
[b]*Department of Physics, Montana State University, Bozeman, MT 59717, USA*
[c]*S2 Corporation, Bozeman, MT 59718, USA*
[d]*University of Colorado, Boulder, CO 80309, USA*

Available online 3 March 2007

Abstract

This paper outlines the efforts to develop an ultra-wideband spectrum analyzer that takes advantage of the broad spectral response and fine spectral resolution (~25 kHz) of spatial-spectral (S2) materials. The S2 material can process the full spectrum of broadband microwave transmissions, with adjustable time apertures (down to 100 μs) and fast update rates (up to 1 kHz). A cryogenically cooled Tm:YAG crystal that operates on microwave signals modulated onto a stabilized optical carrier at 793 nm is used as the core for the spectrum analyzer. Efforts to develop novel component technologies that enhance the performance of the system and meet the application requirements are discussed, including an end-to-end device model for parameter optimization. We discuss the characterization of new ultra-wide bandwidth S2 materials. Detection and post-processing module development including the implementation of a novel spectral recovery algorithm using field programmable gate array technology (FPGA) is also discussed.

PACS: 42.40.Ht; 42.50.Md; 42.79.Hp

Keywords: Spectrum analysis; Spatial spectral holography; Hole burning; Spectral recovery

1. Introduction

There is a growing need for RF spectrum analyzers capable of detecting broadband microwave signals with precision and with millisecond response times. The proliferation of electronic signals in battlefield environments poses a significant challenge to modern defense systems. Emerging electronic support systems must have the capability to detect and respond to multiple electronic signals that can be centered anywhere in the DC to tens of gigahertz range. While sophisticated hardware is available to lock on to signals over the microwave band given the sources center frequency, monitoring the full microwave band for signals of interest poses a major challenge.

Large bandwidth acousto-optic spectrum analyzers [1] relied on diffraction of light by a traveling-wave nature where the angular shift was proportional to RF frequency. The bandwidth is limited by the acousto-optic response times and the diffraction efficiency. Optical spectral hole-burning technology utilizing spatial spectral (S2) materials has been proposed as a solution for performing spectral analysis on short bursts of broadband frequency agile microwave signals. A spectrally multiplexed diffraction analyzer using an electro-optic modulator (EOM) and spatial-spectral holography, that operates analogously to the acousto-optic spectrum analyzer converting spectral content to spatial angle information has been developed [2–4]. The spatial diffraction, however, renders it less suitable to two-dimensional array applications. A novel chirp transform approach has been applied to perform spectral analysis [5,6]. This approach has been shown to provide Fourier transform limited access to the spectrum

*Corresponding author. Tel.: +1 406 994 7675; fax: +1 406 994 6767.
E-mail address: krishna@spectrum.montana.edu (R. Krishna Mohan).

0022-2313/$ - see front matter © 2007 Elsevier B.V. All rights reserved.
doi:10.1016/j.jlumin.2007.02.016

and a record time bandwidth product of 24,000 over a 1.6 GHz bandwidth has been demonstrated [7]. A single channel S2 spectrum analyzer (S2SA) that uses a very simple topology for spectral processing utilizing a single spot in an optical crystal, and is thus amenable to spatially multiplexed array applications has been proposed and demonstrated [8–12]. Capture and analysis of the full power spectrum of broadband RF signals lasting less than a millisecond in different signal environments was demonstrated. Key device features such as wide bandwidth (~GHz), sub-MHz resolution, and short time apertures (hundreds of microseconds) were shown.

In this paper we explore the development and characterization of the S2 technology with optical spectral hole-burning materials to enable full spectral analysis of microwave signals. We discuss the implementation of schemes to perform spectral analysis on a variety of RF signals and demonstrate broad bandwidth operation, high-spectral resolution, large material dynamic range, and low readout latency. We also present the design considerations and the development of subcomponent technologies, including novel materials and other enabling techniques.

2. Principle of operation of S2SA

The core of the S2 technology consists of a material that is capable of recording the power spectrum of an optical signal. S2 crystals typically contain rare earth ions (10^{19} ions per cm^3), such as Thulium (Tm) or Erbium (Er) that are doped into oxides like YAG, a common laser host material. The individual ions doped in the crystal have narrow optical resonances, exhibiting linewidths on the order of a kilohertz at cryogenic temperatures (4–6 K). Due to microscopic inhomogeneities in the crystal, the resonant frequency of each ion is shifted from its nominal value. These shifts are randomly distributed and lead to an inhomogeneous absorption profile that can range from 20 GHz to over 200 GHz wide. The dopant ions can be viewed as a bank of narrow band filters and the S2 materials act intrinsically like multi-channel spectrum analyzers. The narrow homogeneous linewidth of ~kHz gives the S2SA its fine spectral resolution, while the inhomogeneous profile lends itself to the broadband spectral coverage. The ratio of the inhomogeneous bandwidth to the homogeneous linewidth yields the number of spectral channels or the time-bandwidth product of the spectrum analyzer. Ratios as high as 10^8 have been speculated [13] and a huge channel capacity has been demonstrated [7].

The basic components and the principle of operation of the S2SA are shown in Fig. 1. The RF input signal to be analyzed is modulated onto an optical carrier, which is tuned to the resonance wavelength of the ions (Tm −793 nm or Er −1.5 μm) by a high-bandwidth EOM. The optical carrier must have a linewidth less than the device's required frequency resolution. The EOMs facilitate the transfer of the full electronic spectrum to the optical domain. The modulated optical beam illuminates one spatial location on the S2 crystal. If the bandwidth of the modulated optical beam lies within the inhomogeneous absorption profile of the material, then the full power spectrum of the optical beam is recorded through optical spectral hole-burning. Multiple spectral features can be burned independently and simultaneously, where the resultant absorption profile depends on the integrated power or optical energy at each frequency. This recorded power spectrum stored in the modified absorption profile persists for the population lifetime of the absorption transition levels, which is ~10 ms in Tm- and Er-doped crystals.

As shown in the Fig. 1, the power spectrum of the input field is burnt into the S2 material. In the current device configuration, the crystal's modified absorption profile is read out with a frequency scanning optical beam that could be created by modulating either the same laser used in the recording stage or a second independent laser source. The development of readout techniques is described later.

It is illustrative to refer to two theoretical approaches that describe the response of the S2 medium to optical fields. Colice et al. [14] used perturbation theory to describe this interaction and adapted it to the spectrum analysis application by suitably choosing the input fields. S2 medium was treated as a collection of programmable filters, recording the power spectra of the incident signals that determined the filter shape. When a chirp probes the programmed filter, a response is produced whenever the instantaneous chirp frequency correlates with the filter's spectral components. Using slow chirp rate condition, an expression for the output field was obtained (cf. Eq. (12) in Ref [14]) as

$$E_{\text{out}}(t) \propto H(2\pi\kappa t)\mathrm{e}^{-i\pi\kappa t^2}, \tag{1}$$

where H is the transfer function denoting the recorded power spectrum of the incident signal and κ is the chirp rate.

Chang et al. [15,16], developed a formalism that treats the absorption profile, modified due to arbitrary incident signals, as a series of sinusoidal spectral gratings. It is represented by $\alpha(v) = \int_0^\infty \gamma(\tau)\cos[2\pi v\tau + \phi(\tau)]\mathrm{d}\tau$, where $\gamma(\tau)$ is the amplitude of the spectral grating with a period corresponding to $1/\tau$ and $\phi(\tau)$ is the phase of that spectral grating. It was shown that when such a programmed S2 material (optically thin medium of length $\mathrm{d}z$) is probed, the resultant output field is given by

$$E_{\text{out}}(t) = E_{\text{in}}(t) - \mathrm{d}z\int_0^\infty \gamma(\tau)\mathrm{e}^{-i\phi(\tau)}E_{\text{in}}(t-\tau)\mathrm{d}\tau. \tag{2}$$

If a linear frequency chirp is used to read out the power spectrum stored in the material, then the probe pulse of amplitude E_o is represented by $E_{\text{in}}(t) = E_o\cos(2\pi v_s t + \kappa t^2/2)$ where κ is the chirp-rate and v_s is the starting frequency. The output is then shown to be the sum of the delayed weighted chirp echoes from the spectral gratings and the transmitted chirped pulse. The intensity of the readout

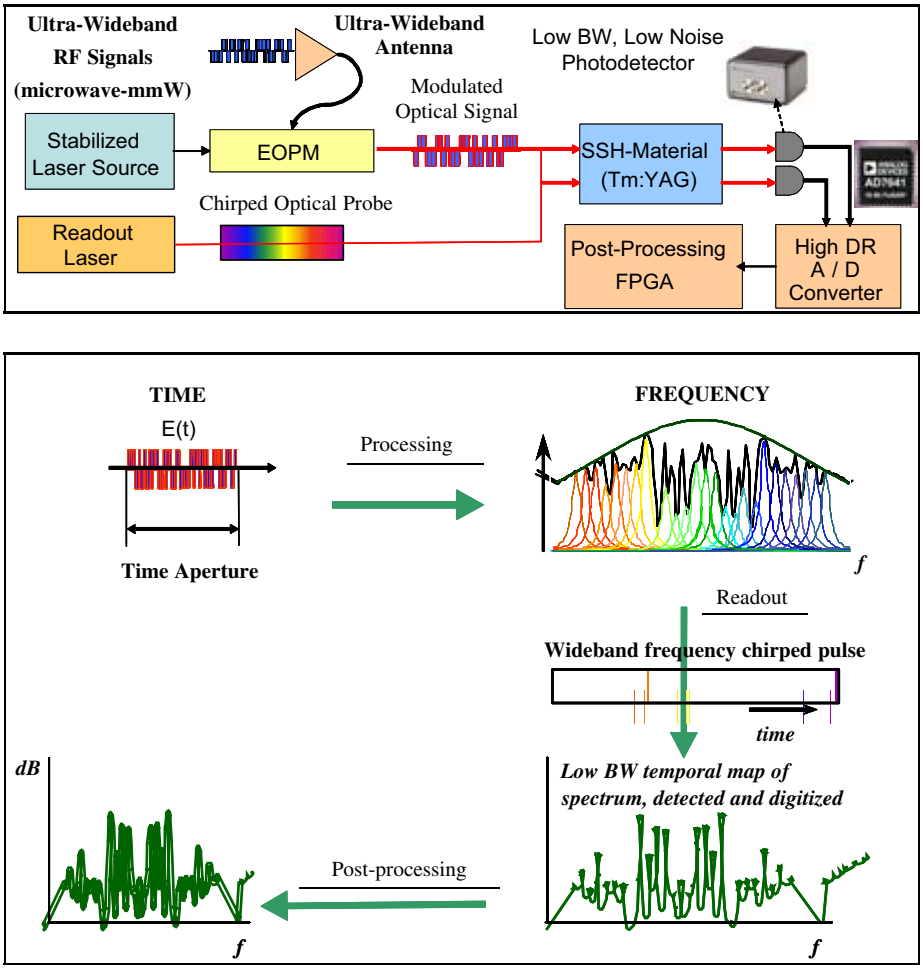

Fig. 1. (Top) Basic components of the spectral analyzer based on optical spectral hole-burning. (bottom) Recording and readout of power spectra of RF waveforms modulated onto an optical carrier. Note that the output bandwidth is dependent on the scan rate.

signal can be obtained as

$$\left|E_{\text{out}}(t)\right|^2 = E_o^2 - 2E_o^2\,\mathrm{d}z \int_0^\infty \gamma(\tau)\cos[2\pi\kappa t\tau + 2\pi\nu_s\tau - \pi\kappa\tau^2 + \phi(\tau)]\mathrm{d}\tau. \quad (3)$$

Under slow scan rate conditions (say $\kappa\tau^2 \ll 1$), the second term of the output is shown to be proportional to $\alpha(\nu)$ with the frequency timescale conversion, $\nu = \kappa\tau$. Thus in either approach, it is observed that for slow chirp rates, the output field is the time domain map of the recorded power spectrum resulting in spectral analysis and that the transformation between coordinate domains is scaled by the chirp rate κ. This implies that the S2SA exhibits a temporal impedance matching capability whereby a multi-gigahertz RF input signal is scaled to low-bandwidth output that depends on the scan rate. Thus the readout signal carrying the desired power spectrum is detected with a low-bandwidth photodetector that enables the use of commercially available inexpensive low sample rate analog-to-digital converters.

A crucial aspect of the device operation is the fast readout of the stored spectral features. The stationarity condition in conventional spectroscopic readout dictates that the spectral resolution ($\Delta\nu$) and the scan rate (κ) are related by $\Delta\nu \approx \sqrt{\kappa}$. Thus a spectral resolution of 100 kHz over 1 GHz bandwidth requires a scan time of 100 ms, which is beyond the limit of the storage time in the S2 materials and also well beyond the desired device latency specification. A consequence of broadband fast scans of narrow spectral features is an oscillatory distortion on the readout feature, observed clearly in Ref. [17] and described in detail in Ref. [15]. The quadratic phase term $\pi\kappa\tau^2$ in Eq. (3) is responsible for the deviation from the direct spectral mapping for fast scans. A novel post-processing algorithm was developed [16] to remove the distortions on the readout spectrum. The limitations on readout latency are overcome by this technique, without sacrificing resolution. Its implementation in a DSP environment is described later.

In some demonstrations discussed below, a dual beam geometry was employed to achieve background subtraction on readout. The chirped probe beam is split before entering the crystal such that, in addition to probing the power spectrum burned in one spatial location, the chirped beam also probes a spot of the crystal that did not experience any

recording. The portion that illuminates the unprocessed location in the crystal acts as a reference and carries the absorptive background information and the other portion reads the spectra and carries the desired spectrum. These beams are incident on a differential detector, operating in a balanced mode that facilitates extraction of the common mode signal. This differential detection scheme enables background subtraction and rejection of laser intensity noise. It should be noted, however, that the shot noise increases with this technique. The basic circuitry of the balanced detector and the principle of operation are detailed in Ref. [18]. The detector used in the experiments described here utilized a pair of Hamamatsu 3883 photodiodes and a linear high-pass response output was used.

3. Experimental demonstrations

Several features of the device were investigated in order to establish the operational phase space and provide guidelines for the prototype device architecture. The investigations ranged from device performance demonstrations such as wide spectral coverage and fine spectral resolution to characterization studies such as material dynamic range. Some results from these investigations are provided in this section.

3.1. Gigahertz bandwidth demonstration—wide spectral coverage

A high-bandwidth proof of concept experiment was performed to demonstrate the ability of the S2SA to capture and process RF signals that span a wide spectrum. The RF signal used to drive the EOPM to encode the 793 nm optical carrier was generated as a 75 MHz square wave modulation on a 2.5 GHz signal. This produces a series of harmonics of the modulating signal on the optical carrier. The microwave spectrum is recorded in a Tm:YAG crystal, cooled to 4 K, and subsequently read out with an optical chirp in a double-sideband (DSB) readout configuration, which is described later.

Fig. 2 shows the microwave spectrum produced by the S2SA and the features up to the 11th harmonic (>3.3 GHz) can be clearly seen. A zoom of the seventh harmonic shows that the feature is resolved to 260 kHz resulting in a time bandwidth product (TBP) of ~4000. The post-processing algorithm was applied for the removal of distortions due to fast readout. This implementation clearly demonstrates the ability of the S2SA to record and analyze spectra of wideband RF signals that offer about 100 μs or less of capture and trace window. The readout signal spanned 1 GHz bandwidth and a 200 kHz resolution was observed over the full operational bandwidth. The spectral coverage demonstrated here was only 3.5 GHz in Tm:YAG, a system that offers >20 GHz bandwidth. Analyses of spectra spanning tens of gigahertz have recently been demonstrated [11,14].

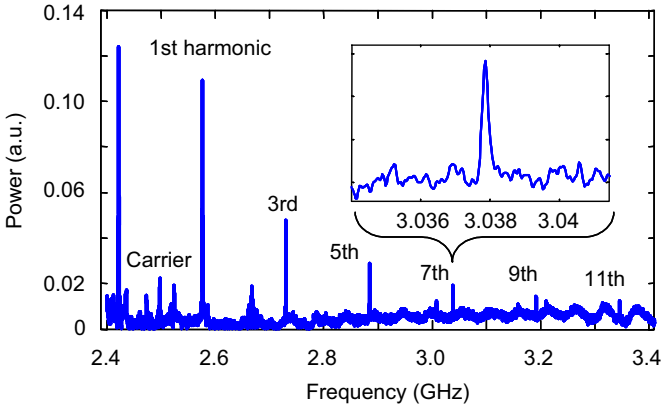

Fig. 2. A single-shot (100 μs) capture and analysis of a microwave RF spectrum up to 3.5 GHz and a zoom of the seventh harmonic showing a 200 kHz resolution using the S2SA.

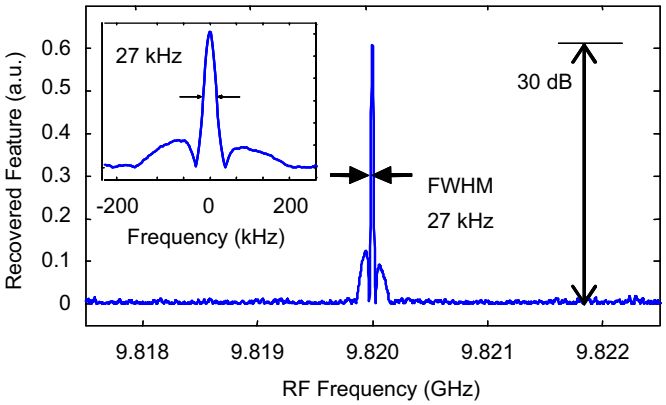

Fig. 3. Resolution of 27 kHz spectral feature on a 10 GHz carrier.

3.2. Ultra-fine spectral resolution on high-frequency RF carriers

This demonstration involves recording and resolving narrow features on RF carriers with frequencies in the X band regime (8–12 GHz). The results from the demonstration of readout of spectrum near 10 GHz are shown in Fig. 3. A remarkable 27 kHz resolution was obtained on the 10 GHz feature, which, to the best of our knowledge, is the narrowest high-frequency feature resolved via hole-burning. The scan rate of 0.1 GHz/ms, used in this demonstration is 100 times over the conventional limit (discussed earlier) required for this ultra-fine resolution. This clearly demonstrates that the readout latency is not bound by the required resolution, a significant benefit in the operation of a practical device. An optical rejection ratio of 1000 is also observed.

3.3. Dynamic range of operation

One of the important device performance specifications is the dynamic range of operation. The dynamic range is typically defined in terms of the minimum detectable

signals, the maximum observable signal before compression, third-order intermodulation (TOI), and other nonlinear mixing terms. We have undertaken a two-fold investigation of the material response to strong RF modulation on optical carriers. The first study is to investigate the relationship between the power of a single RF tone modulating an optical carrier and the depth of the corresponding spectral hole burnt in the S2 medium's absorption profile. It can be shown that the depth of the recorded spectral feature should grow linearly with the recording signal power. However, each spectral bin has a finite number of absorber ions, which leads to the saturation of absorption. Moreover, power broadening causes the spectral features to broaden beyond the desired spectral resolution. These effects affect the dynamic range.

For an arbitrary RF modulation on the optical carrier multiple spectral features at the appropriate frequencies are recorded. Then several factors could hamper the performance of the device. The excitation of ions in the neighboring spectral bins can cause spectral leakage or diffusion leading to cross-talk. The features can blur resulting in loss of resolution. If the powers are high enough to compress the material absorption, nonlinear effects can dominate. The interaction between different spectral components can lead to undesired mixing terms and spurious signals such as TOI affecting the dynamic range of operation. In addition, the presence of a saturating (or jamming) signal could lower the material dynamic range (or sensitivity) for a weaker signal of interest. Such a scenario can be envisaged during real-time spectral surveillance, where strong jammers can mask hostile communications.

To investigate the material dynamic range, the low-bandwidth setup shown in Fig. 1 was employed with an acousto-optic modulator (AOM) to frequency modulate a stabilized laser at 793 nm. Signal generators were used to create the pure RF tones at the desired frequency and create single upper optical sidebands. These features were recorded in a Tm:YAG crystal at 4 K, for a finite interval of time that could be varied by using the AOM as a gate. The recorded features were read out by an optical chirp generated by driving the AOM with an arbitrary waveform generator (AWG). A dual beam set up was employed to perform real-time background subtraction and balanced detection. The readout signals were detected by a photodetector, digitized, and processed to get the feature depth estimate.

3.3.1. Single-tone modulation

A single spectral feature at 265 MHz was recorded in the crystal. The feature was read out with a 10 MHz chirp in 100 μs. The oscillatory readout signal and the recovered feature are shown in Fig. 4. The average peak and the average background were measured. The figure shows the growth of the peak of the output signal with the input RF power.

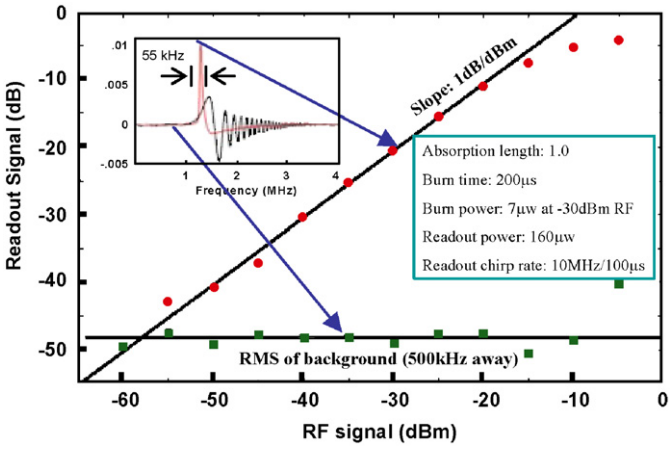

Fig. 4. Material dynamic range at a single spatial spectral location, measured from the peak signal and noise 500 kHz away from the feature. Inset shows the distortion during fast readout and the recovered signal. This data represent an average of several single-shot captures.

It can be seen that the Tm:YAG-based system can be operated with more than 40 dB dynamic range, at a single spectral channel. This can be obtained from the intersection of the two solid lines (1 dB/dBm line and the background noise line) to where the readout signal (dots) deviates from the 1 dB/dBm line. It should be noted that this data represents an average of several single-shot captures. The peak to background ratio in a single capture trace has been observed to be ~30 dB. In this experiment the bandwidth of the spectral feature was around 2 MHz while the detector bandwidth was 15 MHz. In general, the bandwidth of interest for noise considerations is determined by the detector bandwidth, the desired spectral resolution, and the chirp rate even in the wide spectral scan mode of operation.

3.3.2. Two-tone modulation

A two-tone modulation technique to study the nonlinearities and intermodulation in the material revealed that the system presents no intrinsic mixing frequency effects. The study was undertaken in two different ways. The first dealt with varying the power in both the two tones simultaneously and observing the signal strengths at various spectral locations including the tones and the modulation terms. A plot of the growth of the signal power with the RF input power can be seen in Fig. 5(a). The two tones (265 and 266 MHz) maintain the desired linear growth in the signal power till compression similar to the one-tone modulation case. If TOI terms were to exist they should be observable at 264 and 267 MHz. The power at the spectral location corresponding to 267 MHz was monitored along with the noise background 3 MHz away from the tone peak. Both values were statistically identical at the full range of input operational power, thereby demonstrating that no intrinsic temporal mixing effects exist even at saturation.

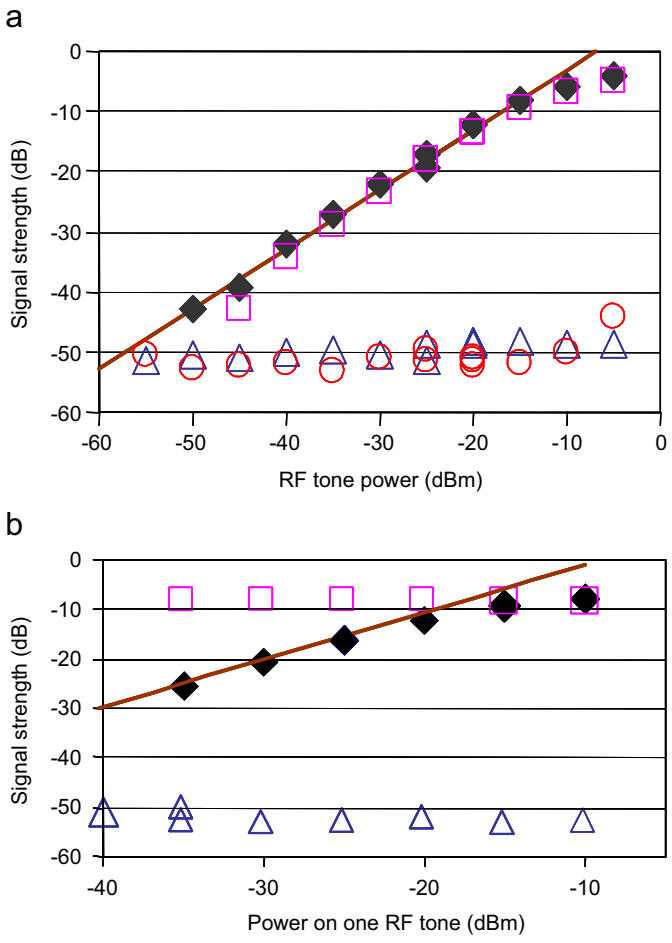

Fig. 5. Two-tone modulation for third-order intermodulation study. (a) Intermodulation, (b) weak tone behavior in the presence of saturating tone. The monitored powers were 265 MHz tone (□), 266 MHz tone (◆), noise (Δ) and the TOI (○). The solid lines show the desired 1 dB/dB slope. All points represent averaged data from several single-shot captures.

The second study deals with the capability of the spectrum analyzer to offer the same dynamic range even in the presence of saturating signals and has applications in operation in extreme environments. In this investigation the power of one of tones (266 MHz) was kept constant while the power on the 265 MHz tone was varied over more than a decade. The results are shown in Fig. 5(b) suggest that S2 devices can discriminate and extract a desired signal that are 40–50 dB lower than a strong saturating signal that is only 1 MHz apart.

The absence of intermodulation terms leads to interesting and significant implications for the device operation. The dynamic range is not limited by spurious signals, or spurs, generated by the material even at compression. Thus the dynamic range is extended into the nonlinear regime of operation. A systematic study of the dynamic range extension is reported in Ref. [14]. The operation of the device in the compression regime is also discussed in the device and subsystem modeling section later.

4. Modular architecture—subsystem development

The above demonstrations clearly show the performance potential of the S2SA device. The specifications for a prototype development were set to reflect these capabilities. Thus, processing bandwidths of 1–10 GHz, spectral resolution of ~25 kHz, recording time aperture, and readout latency of 1 ms, and dynamic range in the interval 30–50 dB were chosen as the target specifications. This section deals with the design, development, and characterization of the subsystems of S2SA to achieve these operational performance specifications. The modular representation of the basic single channel S2SA architecture is shown in Fig. 6. The modules represent a single or a group of subsystems that needed to be developed and interfaced. Other essential modules such as optical amplifiers and spatial multiplexing are not included in this architecture.

4.1. Laser stabilization module

The laser was stabilized using regenerative spectral hole-burning techniques, which allow laser linewidths of ~5 kHz over the 10 ms timescale to be achieved [19]. All the experimental demonstrations in Tm:YAG reported here were carried out with such a stabilized laser source. The linewidth thus obtained also satisfies the requirement that the laser linewidth is smaller than the desired spectral resolution.

4.2. Readout laser module

Here we present a spectral feature readout technique that allows extraction of tens of GHz of spectral information bandwidth at a high resolution. This technique has been employed in most of the experimental demonstrations discussed in this paper and is based upon using a highly coherent master laser [19,20] and applying a linear frequency modulation (LFM) RF waveform to broadband electro-optic phase modulators. This technique, coined DSB readout, though limited in bandwidth sweeping capabililty compared to alterante wideband readout approaches [21], offers spectral resolution comparable to the coherent laser's linewidth (~kHz). As an example this technique can generate over 12 GHz of single-octave LFM bandwidth using a commercially available 40 Gbps pulse pattern generator (PPG) [22]. DSB readout is most applicable when the spectral properties of the recording beam are DSB, which is the case when the input RF is modulated onto a carrier with an EOM.

The electric field of a DSB modulated optical signal can be written as

$$E = E_o \cos(2\pi f_l t + \beta \cos(\pi \kappa t^2 + 2\pi f_s t)), \quad (4)$$

where E_o is the field amplitude, f_l is the unmodulated laser frequency, f_s is the chirp start frequency at $t = 0$ for the first-order sidebands, $\beta = \pi V_o / V_\pi$ is the electro-optic modulation coefficient, V_π is the voltage required to

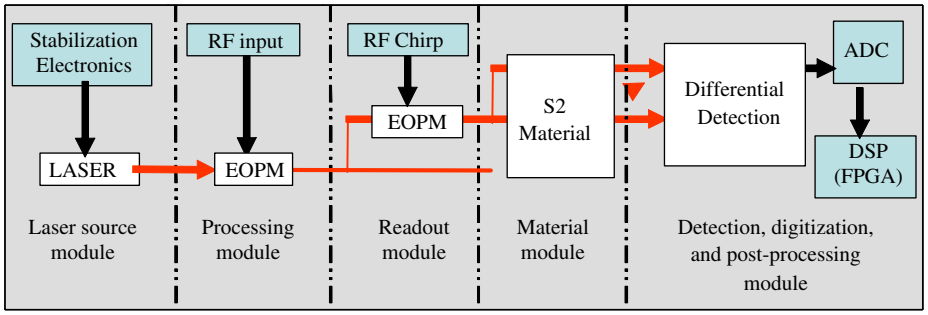

Fig. 6. Modular architecture of the S2SA. The signal pathway used for device model is also shown.

produce a π phase shift, V is the rf driving voltage of the LFM, and κ is the chirp rate defined as $\kappa = \mathrm{BW}/\tau_c$, where BW is the bandwidth for the chirp and τ_c is the chirp time. Eq. (4) can be expanded in terms of Bessel functions as

$$E = E_o \sum_{n=-\infty}^{\infty} J_n(\beta)\cos(2\pi(f_1 - nf_s)t - n\pi\kappa t^2 + n\pi/2). \quad (5)$$

In this form the total electric field can be viewed as a sum of multiple linearly chirping fields, each with a start frequency with respect to the carrier, nf_s, and a chirp rate $n\kappa$ as well as the $n = 0$ optical carrier. The frequency chirped sidebands can be swept linearly (or nonlinearly) in frequency by simply adding the correct time-dependent phase term [23]. Here we assume that the modulator is driven in the linear regime such that only the optical carrier and first-order sidebands are significant. A power spectral density (PSD) representation of the DSB technique is shown in Fig. 7(a).

A theoretical discussion on how spectral features are mapped into time domain signals using chirped sources is detailed in Ref. [15], which also discusses the relationship between the chirp rate and resultant spectral resolution. Here we describe DSB readout through basic absorption spectroscopy. As an example, we consider an S2 material with two lorentzian holes, burned at $\pm\omega_0$ from the laser line center due to an rf at ω_0 being modulated onto a optical carrier at ω_c with an EOM, as shown in Fig. 7(b). The absorption coefficient may be expressed as

$$\alpha(\omega) = \left[1 - \frac{\eta\Delta\omega_{\mathrm{Hole}}^2}{(\omega-\omega_0)^2 + \Delta\omega_{\mathrm{Hole}}^2} - \frac{\eta\Delta\omega_{\mathrm{Hole}}^2}{(\omega+\omega_0)^2 + \Delta\omega_{\mathrm{Hole}}^2}\right]\alpha_0(\omega), \quad (6)$$

where $\eta < 1$ is the hole depth, $\alpha_0(\omega)$ is frequency-dependent unburned absorption coefficient (the inhomogeneous absorption profile) which peaks at α_0, $\Delta\omega_{\mathrm{Hole}}$ is the hole half-width, and ω_0 is the frequency location of the hole(s) from the laser line center. An important symmetry condition for this example is $2\pi f_1 = \omega_c$, i.e. the recording and readout carrier frequencies are the same. This may be achieved in practice by using the same highly coherent laser for both spectral feature recording and DSB readout.

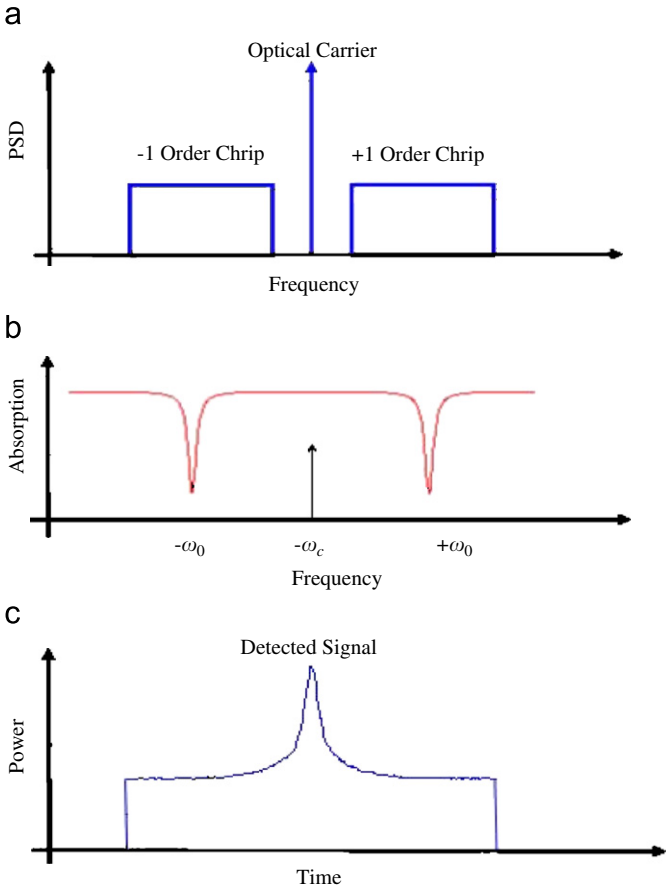

Fig. 7. Schematic of double-sideband readout of spectral holes positioned symmetrically about the laser carrier frequency f_c.

The time-dependent absorption coefficient, according to the above transformation, is

$$\alpha(t) = \left[1 - \frac{\eta(\Delta\tau_{\mathrm{Hole}})^2}{\left(t - (\omega_0/\kappa)\right)^2 + (\Delta\tau_{\mathrm{Hole}})^2} - \frac{\eta(\Delta\tau_{\mathrm{Hole}})^2}{\left(t + [\omega_0/(-\kappa)]\right)^2 + (\Delta\tau_{\mathrm{Hole}})^2}\right]\alpha_0, \quad (7)$$

where the temporal feature width is now $\Delta\tau_{\text{Hole}} = \Delta\omega_{\text{Hole}}/\kappa$ and we have assumed $\alpha_0(\omega) = \alpha_0$ in the region of interest. Since the upper and lower chirp rates are opposite each other, a single temporal hole location is seen at $t_0 = \omega_0/\kappa$.

$$\alpha(t) = \left[1 - \frac{2\eta(\Delta\tau_{\text{Hole}})^2}{(t-t_0)^2 + (\Delta\tau_{\text{Hole}})^2}\right]\alpha_0. \quad (8)$$

This result shows how the time-dependent absorption experienced by the two chirps is identical in time. The detected DSB readout signal, shown in Fig. 7(c), is given by,

$$P_{\text{Det}}(t) \sim P_{\text{read}} \exp(-\alpha(t)L). \quad (9)$$

For the current work, high-bandwidth digital chirp signals were created with a PPG. This is done by using the PPG as if it were an AWG with only 1 bit of vertical resolution. In this situation, the electric field in Eq. (4) is replaced with

$$E = E_o \cos\left(2\pi f_1 t + \phi(t)\right).$$
$$\phi(t) = \begin{cases} \beta & \text{if } \cos\left(\frac{1}{2}\kappa t^2 + 2\pi f_s t\right) > 0 \\ -\beta & \text{if } \cos\left(\frac{1}{2}\kappa t^2 + 2\pi f_s t\right) \leqslant 0. \end{cases} \quad (10)$$

From the well-known sampling theorem [24], any waveform which is bandwidth limited to B_L can be reconstructed from a discrete set of samples taken at a rate $R > R_N$, where $R_N = 2B_L$ is the Nyquist frequency. Thus, assuming a suitably fast sampling rate, the PPG output spectrum is expected to perform well for simple LFM functions, up to the Nyquist limit. We utilized DSB readout using a 12 Gbps PPG to generate 5 GHz sweeps in 200 μs, for a variety of S2-based applications [25]. A generalized readout approach for spectral discovery using multiple frequency-swept sidebands is described in Ref. [25].

4.3. Material module: novel S2 material development

The S2 crystal, which is the core of the device, needs fine resolution and broad spectral coverage. Measurements in Tm:YAG [26] indicated that even under extreme conditions of operation such as high optical or RF power and wide frequency span, 200 kHz spectral resolution was still achievable. The other key requirement for several spectral surveillance applications is ultra-wide bandwidth processing capability. To meet the objective of developing materials for 10 GHz operation scalable to >100 GHz, samples of the novel S2 material, Tm^{3+}:$LiNbO_3$, were fabricated and characterized.

Spectroscopic studies of Tm^{3+}:$LiNbO_3$ have shown that it provides substantial improvements in performance and bandwidth relative to Tm^{3+}:YAG. Polarized absorption and fluorescence spectra between the $^3H_6$ and $^3H_4$ multiplets show that a majority of the transition intensity between the multiplets is concentrated in the lowest-to-lowest $^3H_6(1)$–$^3H_4(1)$ transition of interest for spatial-spectral holography and optical coherent transient applications.

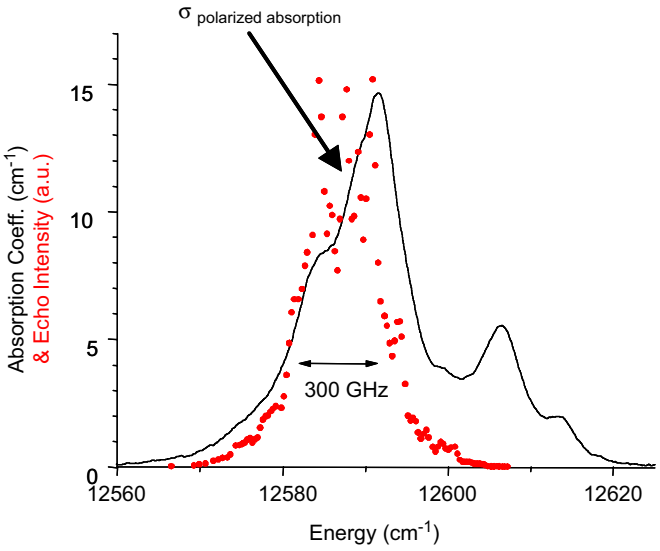

Fig. 8. Absorption coefficient and photon-echo excitation spectrum for the lowest-to-lowest $^3H_6$ (1)–$^3H_4$ (1) transition in 0.1% Tm^{3+}:$LiNbO_3$, showing 300 GHz bandwidth. The large peak 12591 cm^{-1} is the transition of interest. This transition is strongly σ polarized (electric field perpendicular to the *c*-axis).

The σ-polarized $^3H_6(1)$–$^3H_4(1)$ absorption coefficient measured with a thin 0.9 mm thick sample is shown in Fig. 8.

The absorption coefficient for 0.1% Tm^{3+}:$LiNbO_3$ is 15 cm^{-1} compared with 1.7 cm^{-1} for 0.1% Tm:YAG, and the total absorption strength is 250 cm^{-2} compared with 1.6 cm^{-2}. When appropriate factors are considered, the oscillator strength for Tm^{3+}:$LiNbO_3$ is about 50 times larger than that for Tm^{3+}:YAG, making it seven times more sensitive to input signals. The available bandwidth in 0.1% Tm^{3+}:$LiNbO_3$ is 300 GHz (20–30 GHz for Tm:YAG) which was confirmed by measuring the photon-echo-excitation spectrum. These factors combine to provide a surprisingly large increase in material performance.

The homogeneous linewidth Γ_h measured by photon echoes was 25 kHz at 1.6 and 400 kHz at 5.6 K. The temperature dependence of Γ_h from 1.6 to 6.5 K is shown in Fig. 9. Again this is exemplary performance. Using absorption spectra recorded as a function of temperature, we found the second crystal field level at 7.8 cm^{-1}, consistent with the measurements [27]; apparently the electron-phonon coupling is small in this material, resulting in this favorable temperature dependence of homogeneous linewidth. Stimulated photon echo measurements show that the excited state $^3H_4$ lifetime $T_1 = 150$ μs and the bottleneck lifetime is much longer—about 20 ms.

The novel materials described here spectacularly enhance the scalability of the device operation to the 100 GHz range while still yielding sub-MHz spectral resolution.

4.4. Device and subsystem modeling

A simulator of the S2SA was developed that takes into account the operation of the device from RF input through

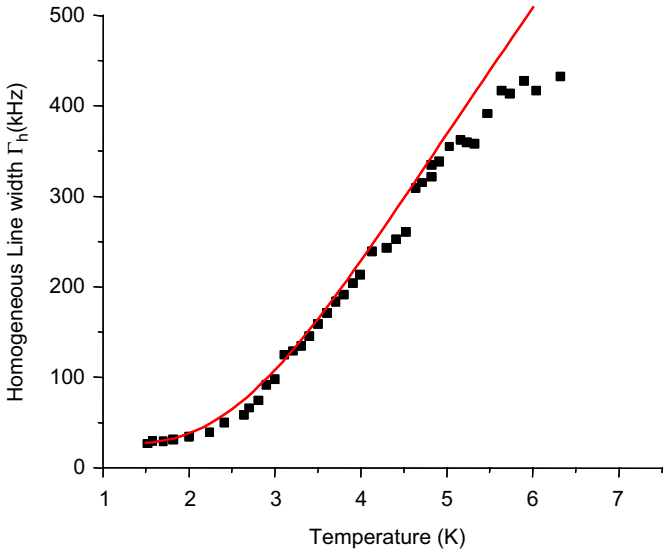

Fig. 9. Temperature dependence of the homogeneous linewidth Γ_h for 0.1% Tm:$LiNbO_3$ measured using two pulse photon echoes as a function of temperature over the range from 1.6 to 6.5 K. The homogenous linewidth is narrower than 500 kHz even at $T = 6$ K, indicating weak coupling to phonons.

the optical chain back to electronic and digital domain and the processed output. Tracking the coupling between signal(s) and noise is useful for monitoring the effects of TOI and saturation, as well as studying the effectiveness of background cancellation techniques. Here we give the details of the simulator along with an example of multitone signal processing.

4.4.1. Time domain signal model

The simulator is a time domain signal model that uses temporal realizations of the signal and noise to track not only the powers of the signal and noise, but the coupling that can occur between them. The simulator tracks the signals and noise from end to end of the device, as can be seen in Fig. 10. The flow of the simulator as well as the effects that are currently included in the simulation are illustrated.

The parameters used in the test simulation are given here. Broadband RF inputs signals are phase modulated ($V_\pi = 2.0$ V) onto an optical carrier (10 mW) at 793 nm to be resonant with Tm:YAG crystal. This optical signal is amplified (gain = 6 dB, noise figure = 3 dB) and incident on the S2 material (0.1% Tm:YAG, 7.6 mm long, absorption length, $\alpha_0 L \sim 1.45$) with a spot radius of 280 μm. The relative intensity noise (−150 dBc/Hz) is included, but the laser linewidth is assumed to be <20 kHz.The incident optical input modifies the absorption profile of the S2 material. The interaction of the input field with the optical medium is done in a manner similar to a PSD analysis, where overlapping segments (64 μs) of the signal are processed in succession for a total observation time of 2 ms. For each segment, the effects of the homogeneous linewidth, set to 20 kHz FWHM, accumulation, incoherent saturation of the absorption, material thickness, the Poissonian nature of the absorption process, and population decay (chosen to be three level in the case of Tm:YAG with a upper state lifetime of 0.8 ms and a 50% branching ratio to a bottleneck state with lifetime of 10 ms) are considered.

The effects of coherent saturation are included, except that rather than compute the exact solution for the saturation due to a modulated pulse (a third-order time-ordered integration over time), the saturation is approximated by a cosine function, whose argument is proportional to the square root of the power spectrum of writing pulse (the pulse area). This simplified algorithm is significantly less computationally demanding but typically leads (depending on temporal structure of writing pulse) to roughly a factor of two overestimation of the total power in all distortions. Since incoherent saturation dominates the coherent saturation, this approximation is not expected to significantly impact SA performance predictions. After the spectrum is recorded, the power spectrum burned in the S2 material is readout with a scanned frequency laser (40 mW laser scanned 200 MHz in 0.2 ms, a scan rate of 1 MHz/μs). During readout, the effects of homogeneous linewidth, detector shot and thermal noise (noise equivalent power (NEP)~3.6 $pW/Hz^{1/2}$), and quantization (16 bits) are taken into account. The 16-bit digitizer is 2 bits greater than required for a 42 dB output dynamic range, but was chosen to better illustrate other noise contributions. The effects of distortion and spectral recovery are not included in the test simulation presented here. The final output is obtained by subtracting the measured signal from a stored signal with zero RF input, which includes a measurement of the fixed fine structure on the inhomogeneous broadened absorption profile due to the limited number of ions in the frequency–space volume of the measurement. Finally, the measured transmission is converted and scaled to the input RF power spectrum to produce the output power spectrum.

To test the dynamic range of the S2SA, the RF input used was made up of 12 tones. Eleven of the tones range from 180 to 280 MHz with 10 MHz spacing. These frequencies were chosen to reduce the computation time of the simulator, but the performance of the device for tone in the multi-GHz range will not change from that predicted here. The 180 MHz tone has an amplitude of 0.8 V (8 dBm in 50 Ω). The rest of the tones are successively 5 dB less, down to −42 dBm at 280 MHz. A tone at 169 MHz is added at 8 dBm to determine the strength of two-tone TOI tone, which would be at 158 MHz. The 8 dBm level was chosen as it produced a two-tone TOI-52 dB down in the optical power spectrum produced by the phase modulator before interaction with the crystal. Fig. 11 shows the digitized power spectrum produced by the S2SA. The output power spectrum was calibrated by setting the tone at 240 MHz to be −30 dB.Thus the figure represents the measure power spectrum relative to the input power level of 8 dBm. A compression of about 10 dB is observed on the

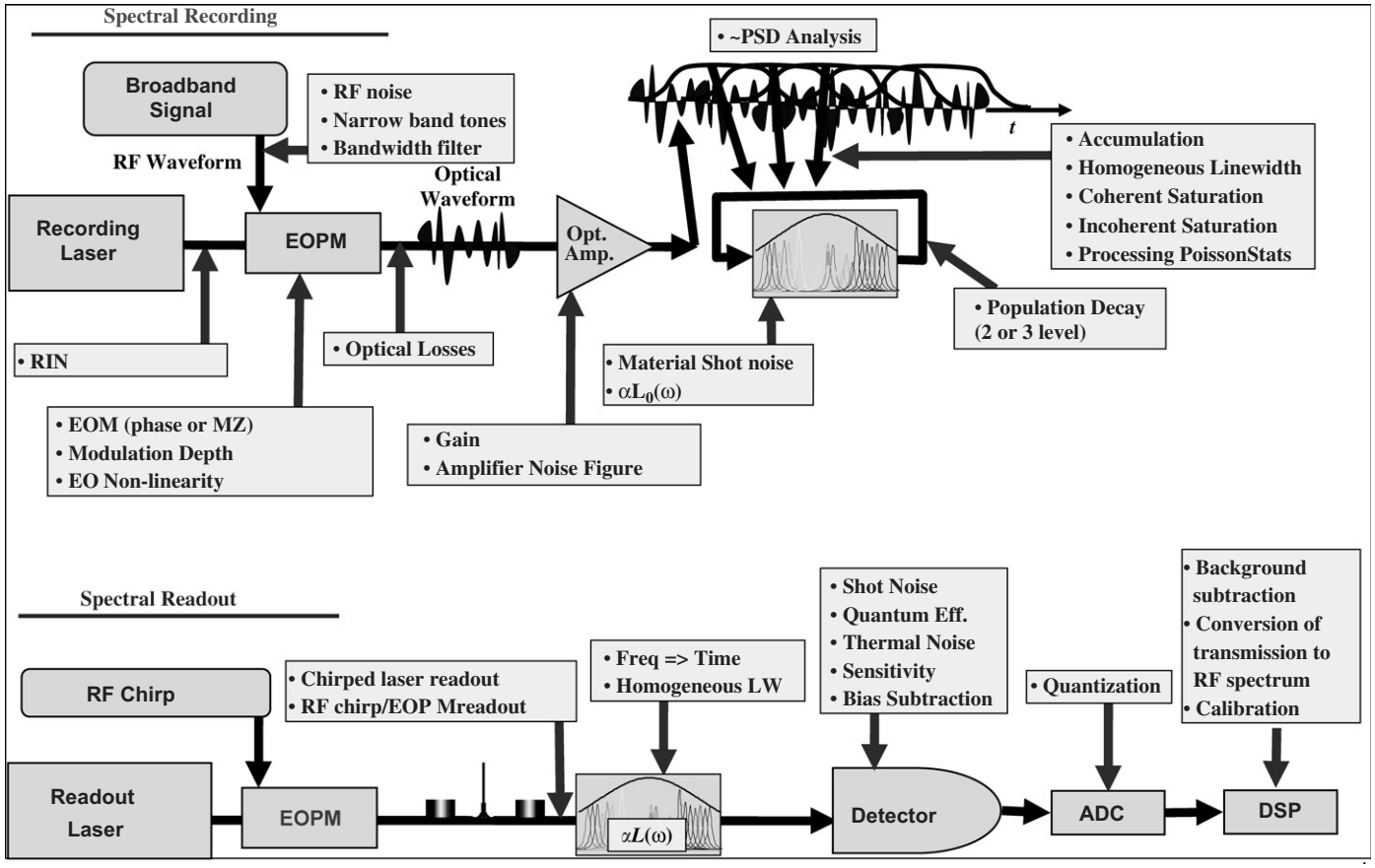

Fig. 10. Schematic of S2SA showing the signal path of the time domain simulator and the effects that are currently included in the simulator, along with those planned to be incorporated.

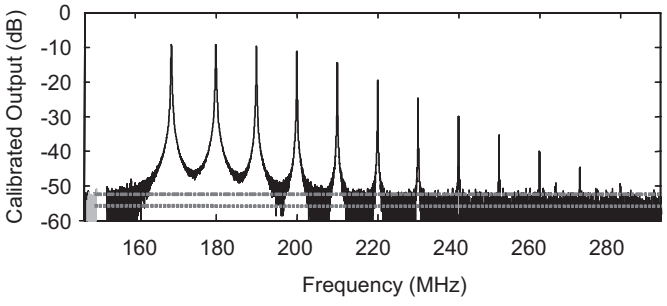

Fig. 11. The measured RF power spectrum produced after detection of the transmission of the read beam and analog-to-digital conversion. The vertical scale is relative to the strongest tone. The dotted line at −55 dB marks the level of the rms noise, which was measured in the region that is shaded gray. The dash-dotted line at −52 dB represents the level of the two-tone TOI.

two strong (8 dBm) tones. The 3 dBm tone at 190 MHz is compressed by 1 dB and all the rest of the tones are within 0.5 dB. The output resolution of 50 kHz was determined by measuring the FWHM of the tone at 210 MHz (−15 dB down from the 8 dBm tones). The dotted line represents the rms noise level of −55 dB, as measured around 152 MHz (the gray-shaded region).

The main contribution to the noise floor is the shot noise of the detected readout signal. The noise floor is proportional to the square root of the readout laser power, but the maximum readout power is limited due to readout saturation. The limit is set by the number of ions in the space–frequency measurement volume. The noise performance of the S2SA can be improved by increasing the spot diameter, along with the recording and read beam powers. Alternative materials could also be used. The −52 dB TOI level is shown with the dash-dot line. The two-tone TOI at 158 MHz due to the two strong tones is barely visible above the noise (<50 dB), illustrating how the TOI of the S2SA system is a consequence of the EOM and not the material interaction. The −48 dB peak seen at 159 MHz is the multi-tone TOI due to all the evenly space input tones and it too is a consequence of the EOM, not the S2 material. The ability of the S2 material to compress the power spectrum without introducing TOI allows it to have a greater than 50 dB input dynamic range, which is well suited to the application of searching for small signals in a sea of strong signals.

5. Module for detection and continuous recovery processing

The back end of the device is the detection and post-processing module that deals with conversion of the optical readout signal into the electronic domain with

photodetectors and subsequent digitization for post-processing to map the spectral features and measure the device dynamic range. Our simulations and experimental results indicate that a typical readout signal consists of a large DC background along with the signal of interest that has an oscillatory distortion, observed when fine spectral features are readout with fast scans. Depending on the depth of the spectrum burned in the absorption profile of the S2 material, the ratio of the signal of interest to the DC background can vary over several orders of magnitude as depicted in Fig. 12.

The problems with the DC component during post-processing are: less gain for signal of interest, digitization errors, distortion, and loss of dynamic range. We designed and tested a single channel biased detection module that could compensate for up to 50 mW of DC optical power. A flat frequency response (DC-60 MHz) at high gain and NEP $\sim$4 pW/Hz$^{1/2}$ were measured. The detector output was digitized for post-processing and used to measure spectral feature shape and depth at high optical powers.

As part of post-processing, a spectral recovery technique has been developed [16] to remove distortions in the output spectra due to fast-chirped readout, as seen in the figure. This can also eliminate the slow chirp rate requirement and lower readout latency. Since recovery is a linear and time invariant filtering operation, it can be performed either in frequency or time domain with an appropriate filter on a digital signal-processing platform. This section deals with the implementation and testing of the continuous real-time spectral recovery algorithm on a digital signal-processing platform based on field programmable gate arrays (FPGA). Continuous real-time recovery is achieved by adapting the original recovery algorithm to an implementation suited for FPGA. Performing recovery in the time domain has the benefit that processing can begin as soon as the readout process starts and the filter only needs to have as many taps as are necessary to obtain a given frequency resolution, thus reducing the processing latency. The details of implementation are described in Ref. [28].

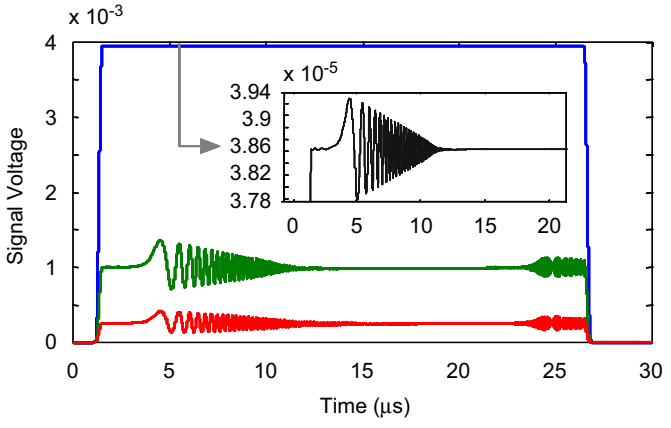

Fig. 12. Typical readout signals showing the signals of interest on a large DC background; the inset shows a zoom of the weak spectrum of interest.

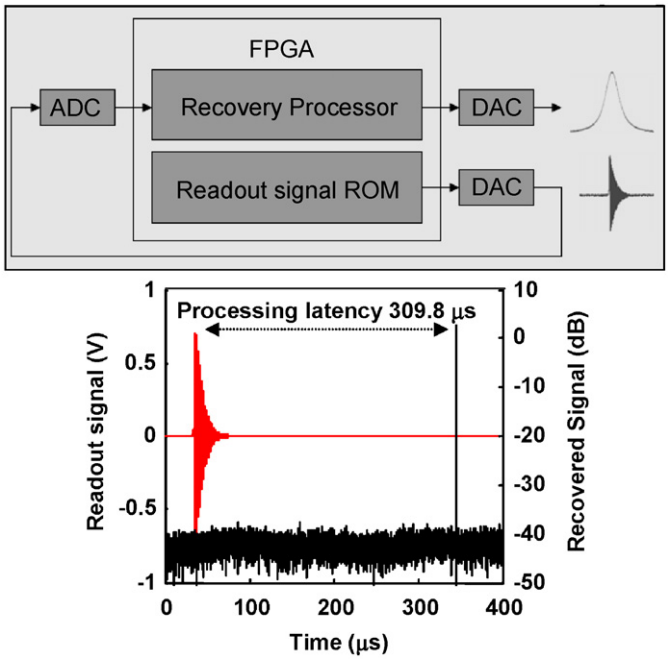

Fig. 13. Setup for recovering a simulated hole readout with FPGA. Oscilloscope captured traces (with averaging) of FPGA performing recovery of a simulated hole (25 kHz) at 1 MHz/μs and sampled at 90 MSPS. The processing latency is 309.8 μs. FWHM of the recovered feature was estimated as 27.8 kHz.

Here we discuss the implementation of this algorithm on an XtremeDSP kit for Virtex-4 manufactured by Nallatech [29]. The kit has dual A/Ds and D/As along with the FPGA core. The algorithm written in VHDL code was programmed into the FPGA core. In a test experiment a simulated readout signal stored in read-only memory (ROM) in the FPGA was used as shown in Fig. 13. This experiment allows for an accurate measurement of processing latency and expected recovered feature width. The ROM stores simulated data representing the ringing due to a 25 kHz wide hole read out at 1 MHz/μs, band-limited to 45 MHz, and sampled at 90 MSPS. In this experiment, the FPGA input also operates at 90 MHz to simulate a hole-burning experiment.

By simultaneously capturing both the readout signal and the recovered signal as shown in Fig. 13 the processing latency has been estimated to be 309.8 μs. This is well within the 1 ms latency limit requirement. By zooming in on the recovered hole, one can make an accurate measurement of the hole-width. The recovery processor achieved a recovered hole-width of 27.8 kHz from reading out a 25 kHz hole at a chirp rate 1 MHz/μs. The width of the hole recovered by the FPGA closely matches the 27.8 kHz width predicted by the simulation when the readout bandwidth is limited to 45 MHz.

In the first real-time demonstration of recovery processing with FPGA-based system a lay out similar to Fig. 1, is chosen. The signal of interest consists of two strong features at 261.8 and 262.2 MHz combined with two

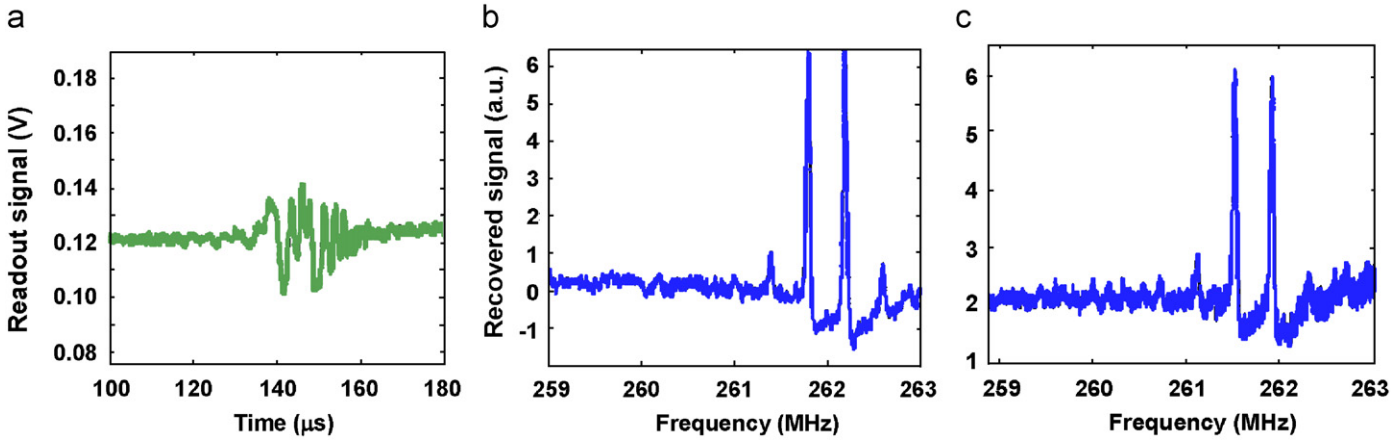

Fig. 14. (a) Readout signal from spectrum with multiple holes. Multiple features read out at 0.05 MHz/μs recovered with the (b) FPGA and (c) Matlab.

weaker features at 261.4 and 262.6 MHz. This signal modulated the laser beam at 793 nm and its spectrum was recorded in Tm:YAG. An AWG produced a linear frequency chirp for readout. The transmitted optical chirp is detected and digitized at 50 MSPS. Reading out the spectrum at 0.05 MHz/μs produced the temporal map plotted as a function of chirp frequency, shown in Fig. 14(a).

Finally, the recovery processor convolved the readout signal with a 4609 tap filter to remove the phase distortion caused by fast readout. The figure also shows the readout signal recovered with the FPGA real-time recovery processor (b) and a Matlab program that performed the frequency domain spectral recovery (c). The strong and weak features are clearly present at the correct frequencies in both recovered spectra, showing that the recovery processor works well for composite spectra. The predicted resolution of ~28 kHz, based on the used FGPA hardware, was observed.

6. Summary

We have described the principle and operation of spectrum analyzer based on S2 materials, which offer the potential for processing and analyzing high-bandwidth analog optical waveforms over arbitrary time apertures. We have demonstrated S2 materials can record and process the power spectra of microwave signals lasting on the order of tens of microseconds and with bandwidths in the tens of gigahertz range, modulated onto an optical carrier. The results of the experimental investigations and the development of subsystem components along with a device simulator have been presented. This device has significant operational and design features. Electronic signals to be analyzed are modulated directly onto an optical carrier with EOMs (phase or amplitude) with no down conversion or multiplexing requirements in the electronic domain. The ability to operate at the RF without any down conversion or demultiplexing in the electronic domain could potentially enhance the spur-free dynamic range (SFDR) of the device. The EOMs facilitate the transfer of the full electronic spectrum to the optical domain and the spectral information is stored in the absorption profile of the S2 material. The S2 material captures the spectrum of the optical signal, through spectral hole-burning, with integration times of 1 μs to 1 ms in a small material volume. A typical spot size ~100 μm, thus 1 cm^2 crystal can simultaneously analyze over 10,000 independent beams. Signals with frequency range within the material absorption band that arrive during the integration time can be intercepted, recorded, and readout resulting in unity probability of intercept. The ability to achieve continuous unity probability of intercept by either allowing continuous exposure of a single spot of the material to the modulated optical signal or employing a two-spot approach with one spot recording while the other is being read out in tandem can also be envisaged.

The authors gratefully acknowledge DARPA and SPAWAR for financial support.

References

[1] R. Schieder, J. Horn, O. Siebertz, C. Mockel, F. Schloder, C. Macke, F. Schmulling, SPIE 3357 (1998) 359.
[2] L. Menager, I. Lorgeré, J.L. Le Gouët, D. Dolfi, J.P. Huignard, Opt. Lett. 26 (2001) 1245.
[3] I. Lorgeré, L. Ménager, V. Lavielle, J.L. Le Gouët, D. Dolfi, S. Tonda, J.P. Huignard, J. Mod. Opt. 49 (2002) 2459.
[4] V. Lavielle, F. De Seze, I. Lorgeré, J.L. Le Gouët, J. Lumin. 107 (2004) 75.
[5] L. Ménager, I. Lorgeré, J.L. Le Gouët, Opt. Lett. 26 (2001) 1397.
[6] V. Crozatier, V. Lavielle, F. Bretenaker, J.L. Le Gouët, I. Lorgeré, IEEE J. Quant. Electron. 40 (2004) 1450.
[7] V. Crozatier, G. Gorju, J.L. Le Gouët, F. Bretenaker, I. Lorgeré, Opt. Lett. 31 (2006) 3264.
[8] R. Krishna Mohan, Z. Cole, R.R. Reibel, T. Chang, K.D. Merkel, W.R. Babbitt, M. Colice, F. Schlottau, K.H. Wagner, in: Proceedings of IEEE Microwave Photonics IEEE, 2004, p. 24.
[9] M. Colice, F. Schlottau, K. Wagner, R.K. Mohan, W.R. Babbitt, I. Lorgeré, J.-L. Le Gouët, in: B. Javidi, D. Psaltis (Eds.), Optical Information Systems II, Proceedings of SPIE, vol. 5557, 2004, p. 132.

[10] F. Schlottau, M. Colice, K.H. Wagner, W.R. Babbitt, Opt. Lett. 30 (2005) 3003.
[11] G. Gorju, V. Crozatier, I. Lorgeré, J.L. Le Gouët, F. Bretenaker, IEEE Photon. Technol. Lett. 17 (2005) 2385.
[12] M. Colice, F. Schlottau, K. Wagner, in: J. Yao (Ed.), Microwave Photonics, Proceedings of SPIE, vol. 5971, 2005, p. 597128.
[13] G.M. Wang, R.W. Equall, R.L. Cone, M.J.M. Leask, K.W. Godfrey, F.R. Wondre, Opt. Lett. 21 (1996) 818.
[14] M. Colice, F. Schlottau, K.H. Wagner, Appl. Opt. 45 (2006) 6393 and references therein.
[15] T. Chang, R. Krishna Mohan, M. Tian, T.L. Harris, W.R. Babbitt, K.D. Merkel, Phys. Rev. A 70 (2004) 063803.
[16] T. Chang, M. Tian, R. Krishna Mohan, C. Renner, K.D. Merkel, W.R. Babbitt, Opt. Lett. 30 (2005) 1129.
[17] L. Ménager, I. Lorgeré, J.L. Le Gouët, R. Krishna Mohan, S. Kroll, Opt. Lett 24 (1999) 927.
[18] P.C.D. Hobbs, Appl. Opt. 36 (1997) 903–920;
P.C.D. Hobbs, Opt. Photonics News 2 (1999) 17.
[19] N.M. Strickland, P.B. Sellin, Y. Sun, J.L. Carlsten, R.L. Cone, Phys. Rev. B 62 (2000) 1463.
[20] For 1.5 μm operation see for example Koheras Corp's Basik laser system.
[21] C. Becker, et al., Opt. Lett 23 (1998) 1194;
L. Menager, et al., Opt. Lett. 25 (2000) 1246;
K. Repasky, et al., Opt. Eng. 42 (2003) 2229;
V. Crozatier et al., Presented at HBSM 2006, submitted to J. Lumin, HBSM 2006 special edition (2006).
[22] See for example, Anritsu Corp's ME7780A.
[23] R.R. Reibel, Z.W. Barber, J.A. Fischer, M. Tian, W.R. Babbitt, J. Lumin. 107 (2004) 103.
[24] B.P. Lathi, Modern Digital and Analog Communication Systems, Oxford University Press, New York, 1998.
[25] Z. Cole, et al., Method and Apparatus for Detecting Optical Spectral Properties using Optical Probe Beams with Multiple Sidebands, US Patent Application # 11/404,549.
[26] K.D. Merkel, R. Krishna Mohan, Z. Cole, T. Chang, A. Olson, W.R. Babbitt, J. Lumin. 107 (2004) 62.
[27] L.F. Johnston, A.A. Ballman, J. Appl. Phys. 40 (1969) 297.
[28] S.H. Bekker, Continuous Real-Time recovery of optical spectral features distorted by fast-chirped readout, Master's Thesis, Montana State University, Bekker_0506, 2006.
[29] See www.xilinx.com—XtremeDSP Development Kit for Virtex 4 (DO-DI-DSP-DK4)